Materials Science & Engineering A 559 (2013) 889–896

Contents lists available at SciVerse ScienceDirect

Materials Science & Engineering A

journal homepage: www.elsevier.com/locate/msea

Effect of welding parameters on microstructure and mechanical properties of friction stir welded Al–Mg–Er alloy

H.L. Hao [a], D.R. Ni [a], H. Huang [b], D. Wang [a], B.L. Xiao [a,*], Z.R. Nie [b], Z.Y. Ma [a]

[a] Shenyang National Laboratory for Materials Science, Institute of Metal Research, Chinese Academy of Sciences, Shenyang 110016, China
[b] College of Materials Science and Engineering, Beijing University of Technology, Beijing 100124, China

ARTICLE INFO

Article history:
Received 23 July 2012
Accepted 12 September 2012
Available online 18 September 2012

Keywords:
Aluminum alloys
Friction stir welding
Microstructure
Mechanical properties

ABSTRACT

3.7 mm thick cold-rolled Al–Mg–Er alloy plates were friction stir welded (FSW) under rotation rates of 400–1200 rpm and welding speeds of 100–400 mm/min. The influence of tool rotation rate and welding speed on the microstructure and mechanical properties were investigated by means of the optical microscope (OM), X-ray diffraction (XRD), scanning electron microscope (SEM), and hardness and tensile tests. Experimental results revealed that defect-free joints could be obtained under a wide range of parameters except for 800 rpm–400 mm/min. The nugget zones (NZs) exhibited equiaxed recrystallized grains and the grain size increased with increasing the tool rotation rate or decreasing the welding speed. For all FSW joints, the NZs exhibited the lowest hardness due to the annealing softening. All the FSW joints fractured in the NZs. The joint welded at 400 rpm–100 mm/min had the greatest ultimate tensile strength (UTS) of 346 MPa and yield strength (YS) of 218 MPa with a joint efficiency of 73%. In general, increasing the tool rotation rate reduced both UTS and YS of the FSW joints, while increasing the welding speed increased UTS and YS.

1. Introduction

Friction stir welding (FSW) is a solid state joining process that uses a rotating tool with a specially designed pin and shoulder inserted into the workpiece [1], and the rotating pin is forced to move along the desired bond line [2]. During welding, friction heating and deformation are produced by the rotating pin and shoulder [3]. The plasticized soft material is transported from the front of the tool to the back that induces significant microstructural changes, including precipitate distribution, texture development and grain size [4,5]. Four different regions, i.e., base material (BM), heat affected zone (HAZ), thermo-mechanically affected zone (TMAZ) and nugget zone (NZ), are identified [6]. Generally, the microstructural changes in various zones have a great effect on the mechanical properties of the weld.

For the FSW joints, the material flow behavior and heat input conditions determine the microstructural evolution in various zones, thereby influencing the mechanical properties of the joints. FSW parameters such as rotation rate, welding speed, tool geometry, and joint design have obvious influences on the material flow and heat input [7]. Among these parameters, the rotation rate and welding speed are the most important parameters that affect the mechanical properties of the joints [8].

Babu et al. [9] reported that increasing the rotation rate or decreasing the welding speed decreased the mechanical properties of FSW 2219Al-T651 joints, while Zhang et al. [10] concluded that the tensile strength of FSW 2219Al-T6 joints increased when increasing the welding speed and was weakly dependent on the rotation rate. Nevertheless, Ren et al. [11] and Feng et al. [12] reported that the tensile strength increased with increasing the welding speed, and it was independent of the rotation rate for FSW 6061Al-T651 joints. Therefore, the effect of the FSW parameters on the joint properties is quite different for various aluminum alloys, and optimizing the FSW parameters is very important for obtaining high-property FSW joints.

Al–Mg alloys are widely used in aerospace and transportation industries because of their low density, high strength to weight ratio, excellent corrosion resistance and good formability [13]. As solution-strengthened alloys, Al–Mg alloys can only be strengthened by working hardening and microalloying [14]. The addition of erbium (Er) element into the Al–Mg alloys can refine the as-cast structure, retard the recrystallization [15] and improve the corrosion resistance [16]. Because of the abundant reserves of Er and its low price, Al–Mg–Er alloys have a wide prospect of development, especially in aerospace and shipbuilding industries [17].

Li [18] welded the cast Al–Mg–Er alloy plates using traditional tungsten inert gas arc welding (TIG) and laser welding (LW) methods. The ultimate tensile strength (UTS) and yield strength (YS) could reach to 80% and 50% of the BM for the TIG joints, and 75% and 60% of the BM for the LW joints, respectively. However,

* Corresponding author. Tel./fax: +86 24 83978630.
E-mail address: blxiao@imr.ac.cn (B.L. Xiao).

0921-5093/$ - see front matter © 2012 Elsevier B.V. All rights reserved.
http://dx.doi.org/10.1016/j.msea.2012.09.041

both fusion welding methods have high requirements for welding preparation and easily result in the welding flaws such as cracks, slag inclusions and distortion. By comparison, there is no need of surface cleaning operations prior to the FSW process and the welding flaw can be avoided [19]. To the best of our knowledge, the effect of welding parameters on the weldability and mechanical properties of FSW Al–Mg–Er joints was not investigated.

In this study, 3.7 mm thick cold-rolled plate of Al–Mg–Er alloy was subjected to FSW investigation at a wide range of parameters. The aim of this study is (a) to evaluate the weldability of the Al–Mg–Er alloy under wide welding parameters and (b) to elucidate the effect of the FSW parameters (rotation rate and welding speed) on the microstructure and mechanical properties of the joints.

2. Experimental procedure

3.7 mm thick cold-rolled plates of Al–4.7Mg–0.6Mn–0.1Zr–0.3Er (wt%) were used in this study. The plates were FSWed along the rolling direction using a FSW machine. A steel tool with a concave shoulder 12 mm in diameter and a threaded cylindrical pin 5 mm in diameter and 3.4 mm in length was used. FSW was conducted at rotation rates of 400–1200 rpm and welding speeds of 100–400 mm/min. A tilting angle of 2.5° was used for all FSW processes and the plunge depth of the shoulder was controlled at ~0.25 mm. FSW parameters used in this study are summarized in Table 1.

In order to reveal the grain microstructure, the FSW samples were first artificially aged at 120 °C for 16.5 h to decorate the grain boundaries and then cross sectioned perpendicular to the FSW direction. The sectioned specimens were polished and then etched with a solution of 10 mL phosphoric acid and 90 mL water at 80 °C. Macrostructure and microstructure of the FSW joints were observed by stereoscopy and optical microscopy. The X-ray diffraction (XRD) was used to determine the second phase particles. The precipitation distribution and the dislocation structures were characterized by the transmission electron microscopy (TEM, TECNAI 20). Thin foils for TEM were prepared by jet electro-polishing with a solution of nitric acid (1/3) and methanol (2/3) at −30 °C.

Vickers hardness profiles were measured on the cross-section perpendicular to the welding direction along the mid-thickness of the plates using a computerized Buehler hardness tester under a load of 100 g for 10 s. Transverse tensile specimens with a gage length of 40 mm and a gage width of 10 mm, as shown in Fig. 1, were machined perpendicular to the FSW direction. Room temperature tensile tests were carried out at a strain rate of $6\times10^{-4}\,s^{-1}$ and three specimens were tested for each condition. The failed tensile specimens were observed using stereoscope and the fracture surfaces were examined on a Quanta 600 scanning electron microscope (SEM).

Table 1
Summary of FSW parameters for cold-rolled Al–Mg–Er alloy plates.

Sample no.	Rotation rate (rpm)	Welding speed (mm/min)
1	400	100
2	800	100
3	800	200
4	800	400
5	1200	100

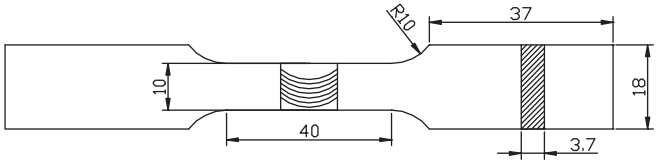

Fig. 1. Dimensions of tensile specimen.

3. Results and discussion

3.1. Macrostructure and microstructure

Fig. 2 shows the cross-sectional macrographs of the FSW joints at different parameters. All the FSW joints consisted of four different regions: BM, HAZ, TMAZ and NZ. The shapes of the NZ were apparently parameter dependent. As shown in Fig. 2(e), generally, the NZ consisted of shoulder-driven zone (SDZ), the pin-driven zone (PDZ) and the swirl zone (SWZ) according to the role of shoulder and pin [10,20].

Onion ring structure was observed at the PDZ of the NZ, and the "line S" (as shown by black arrows) appeared at the SDZ except for Fig. 2(a) where the "line S" was observed from the top to the bottom. The "line S" was believed to originate from the oxide layer on the initial butt surface, which was broken up, extruded and deformed during FSW [21,22]. It is well known that the heat input during FSW decreases with decreasing the rotation rate and increasing the welding speed. Lower heat input condition leads to insufficient break-up of the oxide layer during FSW [23]. This should be the reason why the "line S" was clearer at the parameters of 400–100 mm/min.

During FSW, the material flowed around the tool pin. FSW joints are prone to defects like pinholes, tunnels, cavities, kissing

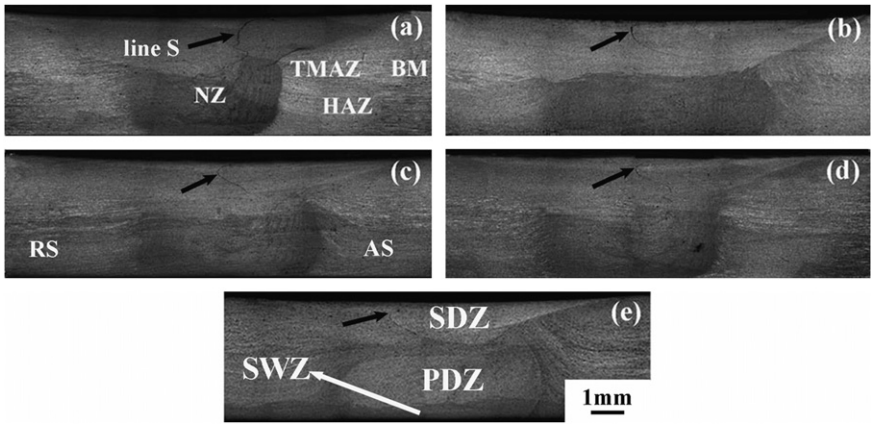

Fig. 2. Cross-sectional macrographs of Al–Mg–Er joints with parameter combinations of (a) 400 rpm, 100 mm/min; (b) 800 rpm, 100 mm/min; (c) 800 rpm, 200 mm/min; (d) 800 rpm, 400 mm/min; and (e) 1200 rpm, 100 mm/min.

bonds, cracks, etc, due to insufficient or excess heat input in the NZ [24,25]. Among the five different FSW parameters used in this study, the parameter of 800 rpm and 400 mm/min resulted in the cavity defect, while defect-free welds were produced at other parameters. The formation of the cavity defect at 800 rpm–400 mm/min was attributed to insufficient heat input and inadequate material flow towards the bottom of the weld [26].

Fig. 3 shows the microstructure of the BM and HAZ near the TMAZ for the FSW joint at 400 rpm–100 mm/min. The grains of the BM were elongated, as shown in Fig. 3(a). Compared to that of the BM, the microstructure of the HAZ which experienced a thermal cycle was significantly coarsened (Fig. 3b). Similar HAZ microstructures were also observed in the FSW joints under other parameters.

From Fig. 4, it is clear that all the NZs consisted of fine-equiaxed grains, indicating the occurrence of dynamic recrystallization in the NZ [27]. At a constant welding speed of 100 mm/min, the grain sizes in the NZs increased from 3.5 to 5.6 μm with increasing the rotation rate from 400 to 1200 rpm (Fig. 4a, b, e). At a constant rotation rate of 800 rpm, there were a little difference in the grain sizes of the NZs for different welding speeds, which were determined to 5.7, 4.8 and 4.7 μm for the welding speeds of 100,

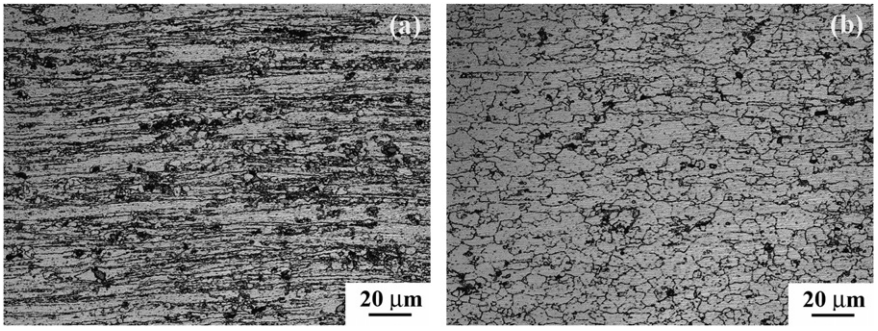

Fig. 3. Microstructures of (a) BM and (b) HAZ near TMAZ at 400 rpm–100 mm/min.

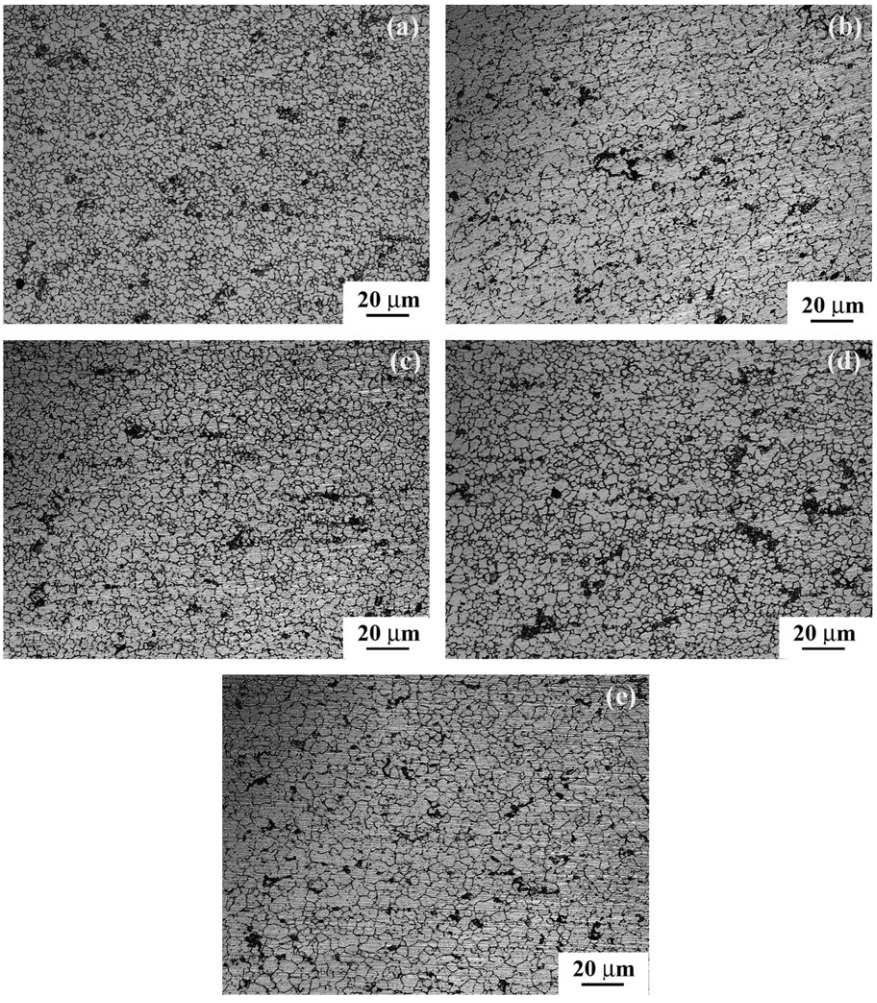

Fig. 4. Microstructures of NZs of FSW joints at (a) 400 rpm–100 mm/min, (b) 800 rpm–100 min, (c) 800 rpm–200 mm/min, (d) 800 rpm–400 mm/min, and (e) 1200 rpm–100 mm/min.

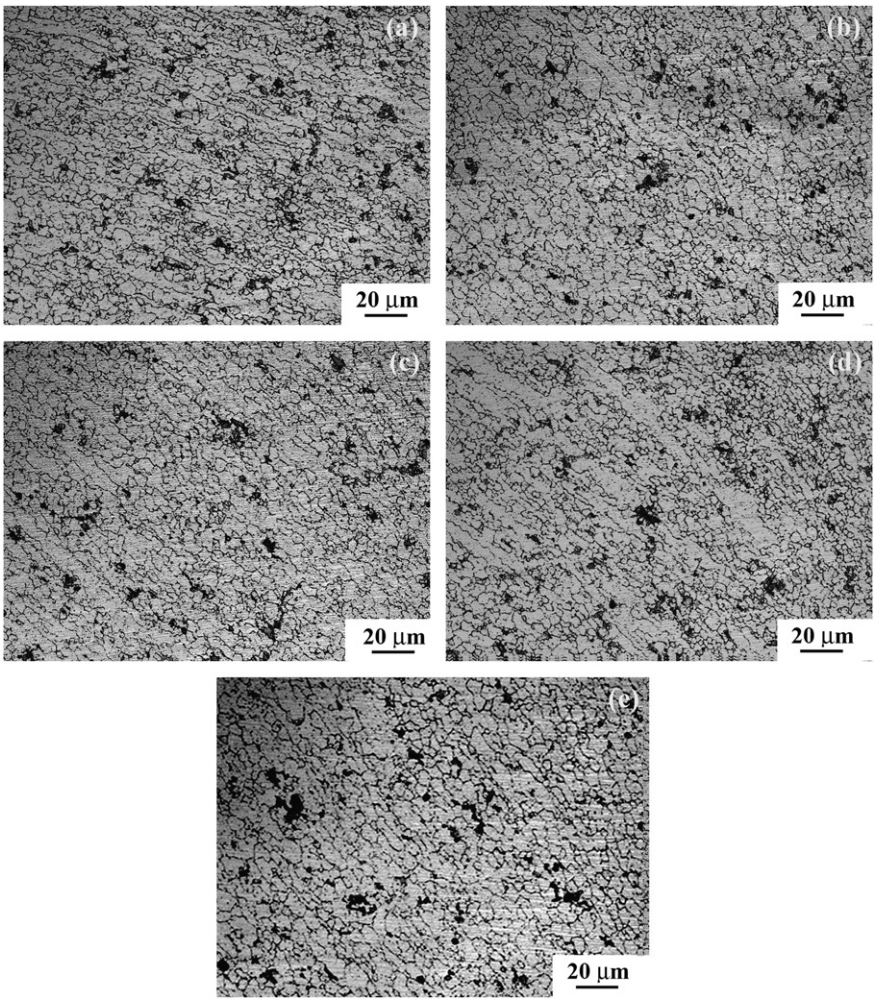

Fig. 5. Microstructures of TMAZs (at retreating side) of FSW joints at (a) 400 rpm–100 mm/min, (b) 800 rpm–100 min, (c) 800 rpm–200 mm/min, (d) 800 rpm–400 mm/min, and (e) 1200 rpm–100 mm/min.

200 and 400 mm/min, respectively (Fig. 4b–d). As shown in Fig. 5, the TMAZs under various FSW parameters were characterized by elongated grains along an upward flowing pattern. This is consistent with previous report [28].

Kim et al. [29] suggested the following equation describing the heat input during FSW process:

$$q = \tfrac{4}{3}\pi^2 \mu P \omega R^3 \tag{1}$$

where q is the heat input, μ is the friction coefficient, P is the pressure, ω is the rotation rate and R is the radius of the shoulder. If the welding speed is considered, Eq. (2) is obtained.

$$Q = \frac{\alpha q}{V} = \frac{4}{3}\pi^2 \frac{\alpha \mu P \omega R^3}{V} \tag{2}$$

where Q is the heat input per unit length, α is the heat input efficiency and V is the welding speed. Because the welding condition is the same, α, μ, P and R are assumed to be constant, and only the W and V are variable. So Q can be expressed by

$$Q = \beta \frac{\omega}{V} \tag{3}$$

where β is a coefficient.

As shown in Eq. (3), increasing the rotation rate or decreasing the welding speed leads to the increase in the heat input. As it is known, higher temperature could lead to the growth of the recrystallization grains. Therefore, with increasing the rotation rate or decreasing the welding speed, the increased heat input resulted in the increase in the size of the recrystallized grains.

Fig. 6 shows the distribution of second phase particles in the BM and the NZs at various welding parameters. It is found that the distribution and size of second phase particles in the NZs of the FSW joints were different from that in the BM. The average sizes of the particles in the NZs were much smaller than those in the BM. This is attributed to the breaking effect of the threaded pin in the NZ [30]. At different FSW parameters, the particles in the NZs were also different. Elangovan et al. [31] considered that at a very high rotation rate, the second phase particles could be broken up sufficiently; at the same time, the particles could be coarsened due to elevated temperature. As the rotation rate increased, the volume fraction of the coarse second phase particles decreased. At a constant welding speed of 100 mm/min, the second phase particles at 1200 rpm were the finest (Fig. 6f). The welding speed also had effects on the distribution and size of the second phase particles (Fig. 6c–e). The volume fraction of the coarse particles decreased when decreasing the welding speed.

Fig. 7 shows the XRD results of the NZs under various FSW parameters. The second phase particles were verified to be Al_3Er, Al_6Mn and Mg_2Si, which were consistent with previous reports [16,32,33]. Fig. 8 shows the dislocations of the BM and NZ. It is clear that the density of dislocations in the NZ decreased dramatically compared to that in the BM, attributable to annealing effect and dynamic recrystallization in the NZ.

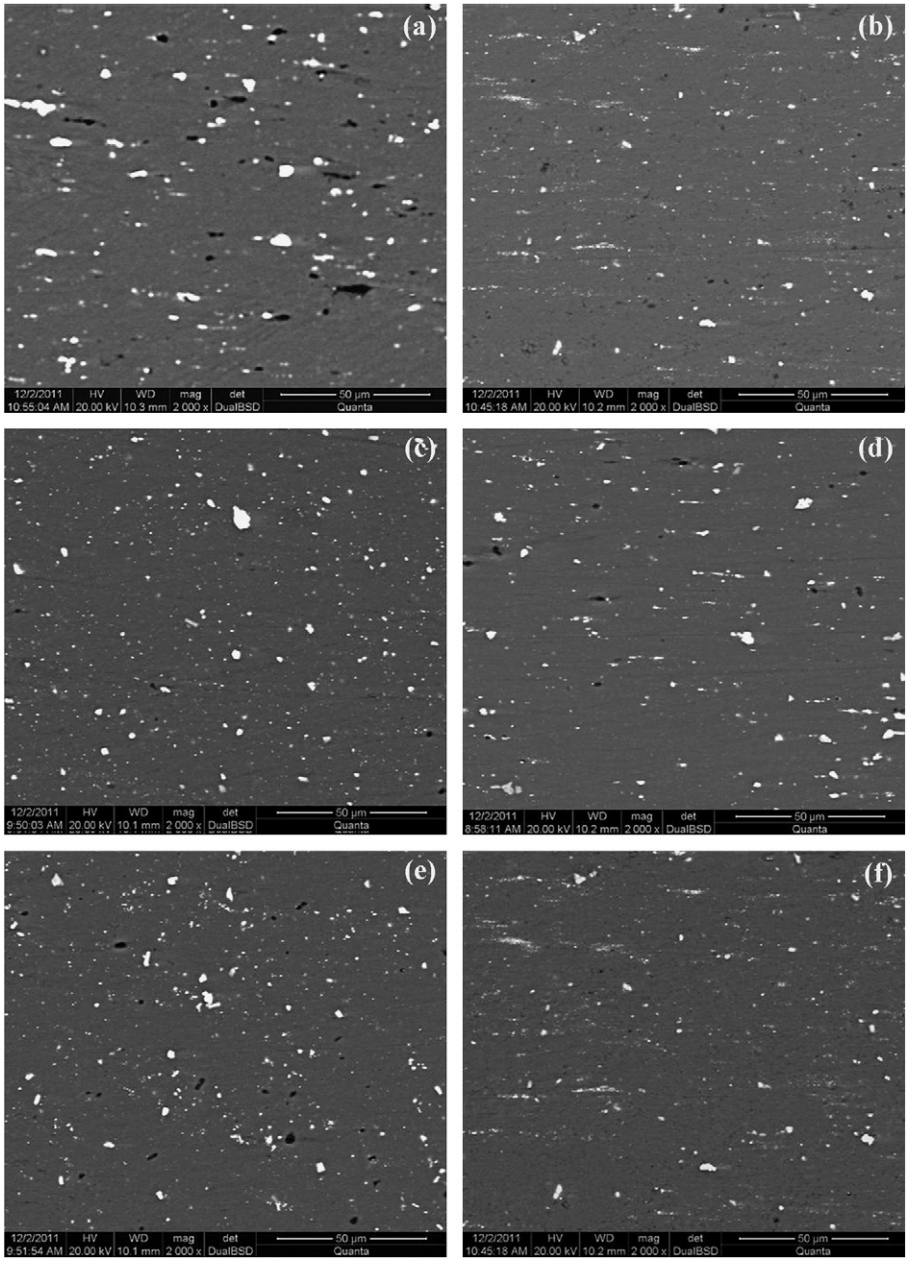

Fig. 6. Microstructures of (a) BM and (b)–(f) NZs of FSW joints: (b) 400 rpm–100 mm/min, (c) 800 rpm–100 mm/min, (d) 800 rpm–200 mm/min, (e) 800 rpm–400 mm/min, and (f) 1200 rpm–100 mm/min.

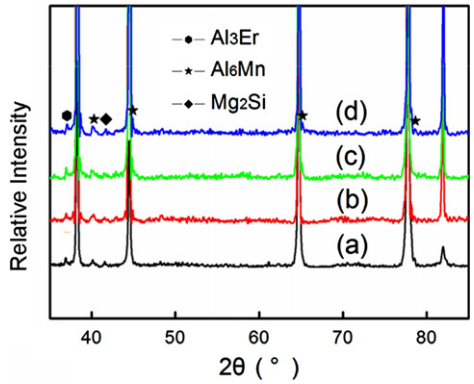

Fig. 7. XRD patterns of (a) BM and (b)–(d) NZs: (b) 400 rpm–100 mm/min; (c) 800 rpm–100 mm/min; and (d) 800 rpm–400 mm/min.

3.2. Hardness profile

Fig. 9 shows the hardness profiles of the FSW joints along the mid-thickness of the transverse section at different parameters. Following observations can be made. First, all welded joints exhibited significantly reduced hardness in the welded zone compared to the BM, which was attributed to the annealing softening and recrystallization [33]. It is known that the cold-rolled aluminum plates exhibited higher hardness due to the work hardening effect. During FSW, the NZ experienced intense plastic deformation and thermal exposure with the peak temperatures up to 0.6–0.95 T_M [27]. Therefore, significant annealing softening and recrystallization occurred [34], leading to significantly reduced hardness value in the welded zone than that of the BM. Second, when increasing the rotation rate from 400 to 800 rpm, the softened region became wider and the average hardness values

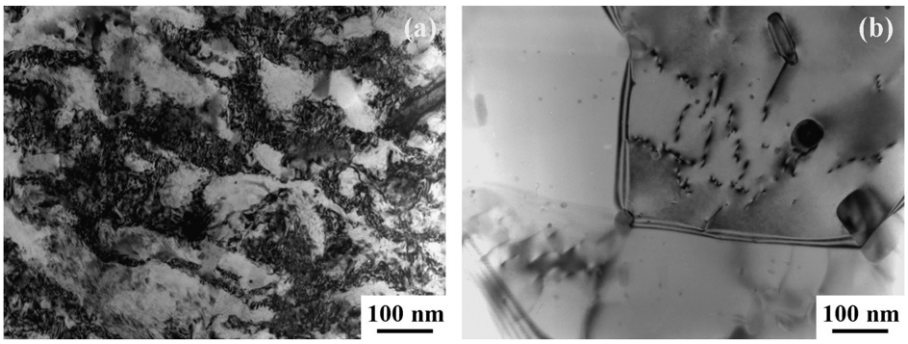

Fig. 8. Bright filed TEM micrographs showing the dislocation structures: (a) BM; (b) NZ at 400 rpm–100 mm/min.

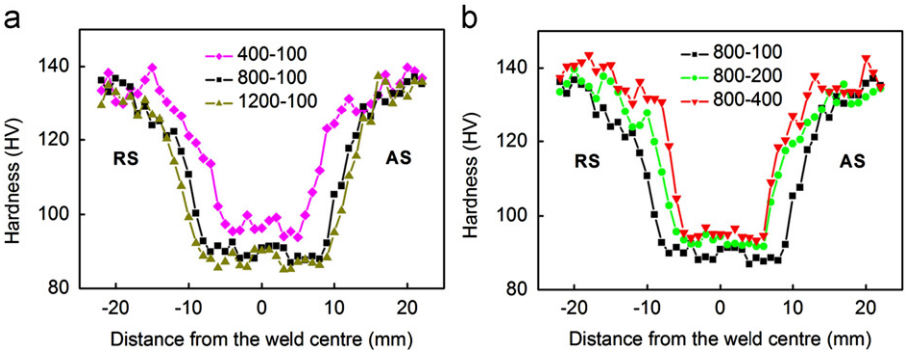

Fig. 9. Hardness profiles at (a) a constant welding speed of 100 mm/min and (b) a constant rotation rate of 800 rpm.

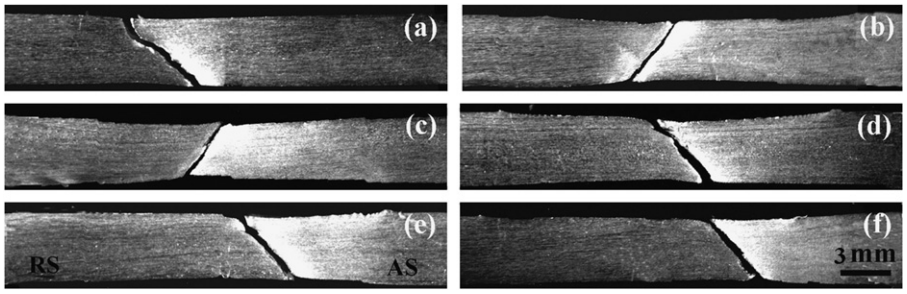

Fig. 10. Failed tensile specimens: (a) BM, (b) 400 rpm–100 mm/min, (c) 800 rpm–100 mm/min, (d) 800 rpm–200 mm/min, (e) 800 rpm–400 mm/min, and (f) 1200 rpm–100 mm/min.

of the welded zone decreased from 100 to 90 Hv (Fig. 9a). However, increasing the rotation rate from 800 to 1200 rpm produced little change to the width of softened region and the average hardness value of the welded zone. Third, at a constant rotation rate of 800 rpm, higher the welding speed, narrower the softened zone was (Fig. 9b). The hardness of the welded zone increased from 90 to 95 Hv when increasing the welding speed from 100 to 200 mm/min. However, the average hardness of the welded zone at 400 mm/min was nearly the same as that at 200 mm/min. The variation trend in the hardness kept pace with the change of the grain size in the NZs. According to the Hall–Petch relationship [31], the larger grain size results in lower hardness.

Fig. 10 shows the fracture location of the BM and FSW joints at different parameters. All the FSW joints fractured in the NZs, where the lowest hardness was achieved, as shown in Fig. 9. Both the BM and the FSW joints exhibited a shear fracture mode, and the shear fracture path was oriented at an angle of about 45° to the tensile axis. Comparing Figs. 2 and 10, it is noted that the fracture of the joints did not occur along the "line S", suggesting that the mechanical properties and fracture behavior of the FSW Al–Mg–Er joints were not affected by the "line S" under the investigated FSW parameters.

Table 2
Transverse tensile properties of FSW Al–Mg–Er alloy joints at room temperature.

Sample	YS (MPa)	UTS (MPa)	Elongation (%)	Joint efficiency (%)
Base metal	409.2 ± 7.6	473.8 ± 0.7	10.1 ± 0.6	
1	218.4 ± 3.6	346.1 ± 0.8	10.0 ± 0.7	73.1
2	182.5 ± 2.1	333.1 ± 1.8	12.6 ± 0.5	70.3
3	195.2 ± 3.8	337.0 ± 1.2	13.1 ± 1.5	71.1
4	196.5 ± 1.7	336.2 ± 1.2	10.2 ± 0.9	71.0
5	181.0 ± 2.3	331.9 ± 2.4	11.7 ± 0.7	70.1

3.3. Tensile properties

Tensile properties of the BM and the FSW joints are listed in Table 2. Three findings were observed. First, there was a significant reduction in the YS and UTS of the FSW joints compared to those of the BM. For all FSW parameters, the joint efficiency was about 70%. Second, at a constant welding speed of 100 mm/min, the YS and UTS of the joint welded at 400 rpm were 218 and 346 MPa, respectively, which were higher than those at 800 and 1200 rpm. The YS and UTS values at these two parameters (800 and

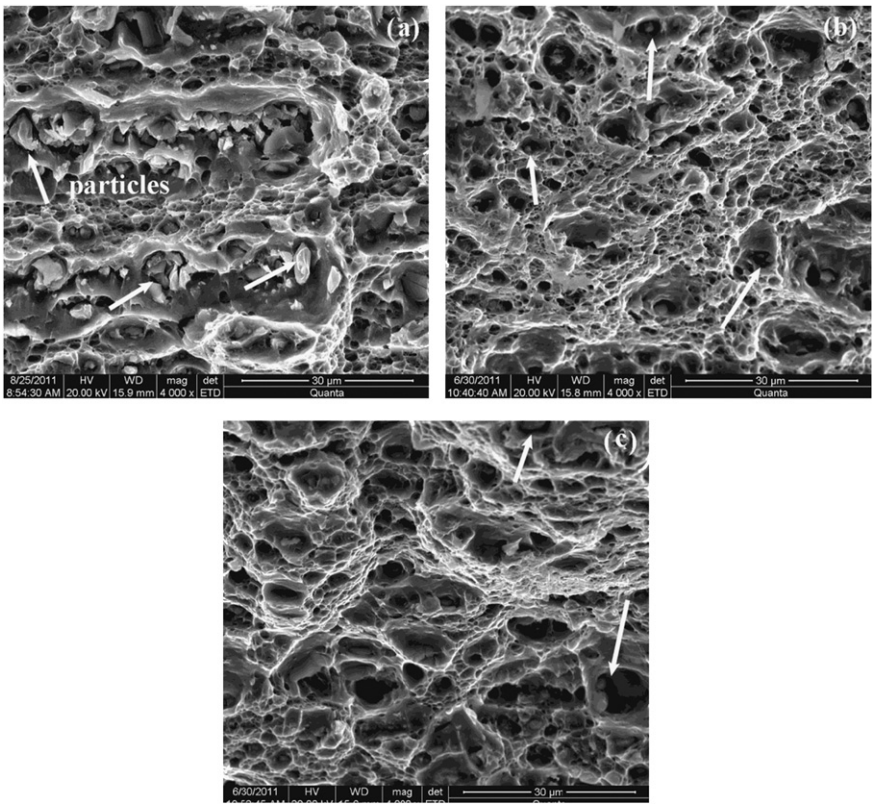

Fig. 11. SEM fractographs of (a) BM (b), (c) FSW joints: (c) 400 rpm–100 mm/min, and (d) 800 rpm–100 mm/min.

1200 rpm) were the same. Third, for the joints welded at a rotation rate of 800 rpm, the YS and UTS at 100 mm/min were lower than those at 200 and 400 mm/min. The YS and UTS values at 200 and 400 mm/min were nearly the same. The elongation at 400 mm/min was lower compared to that at 100 and 200 mm/min. The change of YS and UTS at different FSW parameters was consistent with that of the hardness profiles of the FSW joints.

Scheider et al. [35] and Li et al. [36] reported that the existence of the onion ring did not affect the properties of the weld joints. Sato et al. [21] and Ren et al. [22] thought that the "line S" was composed of broken oxide particles, and such broken oxide particles were dispersed along the fine equiaxed grain boundaries. The distribution of the broken oxide did not form a continuous oxide band in the joint. Therefore, the presence of the oxide particles did not affect the tensile properties of the welded joint.

3.4. Fracture surface

Fig. 11 shows the fracture surface of the BM and the FSW joints welded at 100 mm/min with rotation rates of 400 and 800 rpm. All of the fracture surfaces consisted of dimples with varying size and shape, which indicated that the mode of failures was basically ductile in nature [37]. Comparing the fracture surfaces of the BM with that of welded joints, it was found that the fracture surface of the FSW Al–Mg–Er joints was characterized by fine and round equiaxed dimples, with a few small particles being detected in some large dimples, and tearing edges (Fig. 11c and d). The dimples on the fracture surface of the BM were inhomogeneous and contained more and larger second phase particles and that of the joints had finer second phase particles, which were consistent with that larger second-phase particles were observed in the BM (Fig. 6a) and finer second phase particles in the NZ (Fig. 6b and c).

4. Conclusions

1. 3.7 mm thick cold-rolled Al–Mg–Er alloy plates were joined by FSW at rotation rates of 400–1200 rpm and welding speeds of 100–400 mm/min. The "line S" and onion ring were observed in the NZs for various welding parameters.
2. FSW produced a fine equiaxed grain structure in the NZ. The size of the grains in the NZ increased with increasing the rotation rate from 400 to 1200 rpm or decreasing the welding speed from 400 to 100 mm/min.
3. The FSW joints exhibited significantly softened welded zones. As the rotation rate increased from 400 to 800 rpm, the hardness of the NZ decreased, increasing the rotation rate to 1200 rpm did not reduce the hardness value further. When increasing the welding speed from 100 to 200 mm/min, the hardness of the NZ increased, however, the hardness at 400 mm/min was nearly the same as that at 200 mm/min.
4. The YS and UTS of the FSW Al–Mg–Er joints were reduced compared to those of the BM and all the FSW joints failed in the NZs with a shear fracture, which was consistent with the hardness profiles of the joints. The "line S" did not influence the mechanical properties and fracture behavior of the joints.
5. At a lower rotation rate of 400 rpm, higher YS and UTS were obtained. The YS and UTS values decreased as the rotation rate increased from 400 to 800–1200 rpm. Increasing the welding speed from 100 to 200–400 mm/min led to an increase in the YS and UTS of the joints. The variation trend in the YS and UTS of the joints with the FSW parameters was consistent with that in the hardness in the NZ.

References

[1] K.V. Jata, S.L. Semiatin, Scr. Mater. 43 (2000) 743–749.
[2] R.S. Mishra, Z.Y. Ma, Mater. Sci. Eng. R 50 (2005) 1–78.

[3] Y.S. Sato, H. Kokava, K. Ikeda, M. Enomoto, S. Jogan, T. Hashimoto, Metall. Mater. Trans. A 32 (2001) 941–948.
[4] R.K.R. Singh, C. Sharma, D.K. Dwivedi, N.K. Mehta, P. Kumar, Mater. Des. 32 (2011) 682–687.
[5] Y.S. Sato, H. Kokava, Metall. Mater. Trans. A 32 (2001) 3023–3031.
[6] K. Elangovan, V. Balasubramanian, Mater. Des. 29 (2008) 362–373.
[7] A.M. Mahmoud, T.A.Khalifa Gaafer, Mater. Sci. Technol. 24 (2008) 553–559.
[8] P. Xue, G.M. Xie, B.L. Xiao, Z.Y. Ma, L. Geng, Metall. Mater. Trans. A 41 (2010) 2010–2021.
[9] S. Babu, K. Elangovan, V. Balasubramanian, M. Balasubramanian, Met. Mater. Int. 15 (2009) 321–330.
[10] Z. Zhang, B.L. Xiao, Z.Y. Ma, J. Mater. Sci. 47 (2012) 4075–4086.
[11] S.R. Ren, Z.Y. Ma, L.Q. Chen, Scr. Mater. 56 (2007) 69–72.
[12] A.H. Feng, D.L. Chen, Z.Y. Ma, Materi. Sci. Forum 618-619 (2009) 41–44.
[13] C.Z. Zhou, X.Q. Yang, G.H. Luan, Mater. Chem. Phys. 98 (2006) 285–290.
[14] C.Z. Zhou, X.Q. Yang, G.H. Luan, Scr. Mater. 53 (2005) 1187–1191.
[15] Z.B. Xing, Z.R. Nie, J.X. Zou, X.L. Ji, X.D. Wang, Mater. Sci. Forum. 546–549 (2007) 899–904.
[16] F. Rosalbino, E. Angelini, S.D. Negri, A. Saccone, S. Delfino, Intermetallics 11 (2003) 435–441.
[17] Z.G. Wu, M. Song, Y.H. He, Mater. Sci. Eng. A 504 (2009) 183–187.
[18] C.Y. Li, Beijing University of Technology, Master Thesis (2010) 1–82.
[19] A.A.M. da Silva, E. Arruti, G. Janeiro, E. Aldanondo, P. Alvarez, A. Echeverria, Mater. Des. 32 (2011) 2021–2027.
[20] Z. Zhang, B.L. Xiao, D. Wang, Z.Y. Ma, Metall. Mater. Trans. A 42 (2011) 1717–1726.
[21] Y.S. Sato, F. Yamashita, Y. Sugiura, S.H.C. Park, H. Kokawa, Scr. Mater. 50 (2004) 365–369.
[22] S.R. Ren, Z.Y. Ma, L.Q. Chen, Mater. Sci. Eng. A 479 (2008) 293–299.
[23] Y.S. Sato, H. Takauchi, S.H.C. Park, Hiroyuki Kokawa, Mater. Sci. Eng. A 405 (2005) 333–338.
[24] H.B. Chen, K. Yan, T. Lin, S.B. Chen, C.Y. Jiang, Y. Zhao, Mater. Sci. Eng. A 433 (2006) 64–69.
[25] M. Jayaraman, R. Sivasubramanian, V. Balasubramanian, S. Babu, Met. Mater. Int. 15 (2009) 313–320.
[26] R. Nandan, T. DebRoy, H.K.D.H. Bhadeshia, Prog. Mater. Sci. 53 (2008) 980–1023.
[27] L. Fratini, G. Buffa, Int. J. Mach. Tools Manuf. 45 (2005) 1188–1194.
[28] T.R. McNelley, S. Swaminathan, J.Q. Su, Scr. Mater. 58 (2008) 349–354.
[29] Y.G. Kim, H. Fujii, T. Tsumura, T. Komazaki, K. Nakata, Mater. Sci. Eng. A 415 (2006) 250–254.
[30] J Yang, B.L. Xiao, D. Wang, Z.Y. Ma, Mater. Sci. Eng. A 527 (2010) 708–714.
[31] K. Elangovan, V. Balasubramanian, Mater. Sci. Eng. A 459 (2007) 7–18.
[32] M.M. Attallah, C.L. Davis, M. Strangwood, J. Mater. Sci. 42 (2007) 7299–7306.
[33] Y.S. Sato, S.H.C. Park, H. Kokawa, Metall. Mater. Trans. A 32 (2001) 3033–3042.
[34] Y.Y. Peng, Z.M. Yin, X.F. Lei, Q.L. Pan, Z.B. He, Rare Metall. Mater. Eng. 40 (2011) 201–205.
[35] J.A. Scheider, A.C. Nunes, Metall. Mater. Trans. B 35 (2004) 777–783.
[36] Y. Li, L.E Murr, J.C. McClure, Scr. Mater. 40 (1999) 1041–1046.
[37] N.T. Kumbhar, S.K. Sahoo, I. Samajdar, G.K. Dey, K. Bhanumurthy, Mater. Des. 32 (2011) 1657–1666.